Research Article

Kazuma Kurihara*, Ryohei Hokari and Koji Miyake

Particle size and polymer formation dependence of nanostructure in antireflective surfaces by injection molding process

https://doi.org/10.1515/aot-2019-0018
Received February 5, 2019; accepted April 1, 2019

Abstract: The effects of nanomolding characteristics on an antireflective surface fabricated via injection molding were investigated. The optical property of a sub-wavelength structure (SWS) of our own making was also measured. The sizes of nanostructures fabricated on SWS molds were controlled by changing the average particle diameters used as mask and the time of reactive ion etching. The maximum filling ratio of the injected polymer was increased from 51.7% to 90.4% by changing the average particle diameters from 83.8 nm to 111.2 nm. In addition, the filled ratio of the injected polymer was increased from 51.7% to 73.7% under the same processing conditions. The results of the measurements of the optical property indicated that the reflectance of small-sized and large-sized SWSs fabricated with the same process condition was decreased at the wavelengths of 550 nm and 980 nm, respectively. The wavelength showed that the minimum reflectance was varied from the visible range to the near-infrared range by changing the size of the SWS under the same processing condition. This result led us to conclude that we can obtain antireflection surfaces for any wavelength by varying the size of the SWS under the same injection-molding condition.

Keywords: antireflection; injection molding; mould; nanoimprint; nanoparticle; nanostructure.

***Corresponding author: Kazuma Kurihara,** National Institute of Advanced Industrial Science and Technology (AIST), Tsukuba East, 1-1-1 Namiki, Tsukuba 305-8564, Japan,
e-mail: k.kurihara@aist.go.jp
Ryohei Hokari and Koji Miyake: National Institute of Advanced Industrial Science and Technology (AIST), Tsukuba East, 1-1-1 Namiki, Tsukuba 305-8564, Japan

1 Introduction

Antireflective coatings have been widely employed in applications with optical components, screen displays, high-emission light-emitting diodes (LEDs), and solar cells [1–5]. They commonly consist of multi-layered thin films of dielectric materials deposited by vacuum coating. Depending on the optical performance requirements, the number of multi-layers can be manipulated. An alternative method for antireflective coating of sub-wavelength structures (SWSs) is expected to allow excellent antireflective properties with broad wavelength and incident angle ranges [2, 6]. When the structure feature sizes are less than the incident wavelength, the incident light is not diffracted. The effective refractive index of an SWS is determined by the area ratio of the dielectric material. Depending on the height and the effective refractive index of the SWSs, the cancelation wavelength is determined [7]. Thus, SWSs show antireflection properties in single layers [8–12]. These structures were fabricated by fine pattering processes such as electron beams [13], deep ultraviolet (UV), extreme UV interference lithography [14], and the block copolymer self-assembly of polystyrene (PS)-poly(methyl methacrylate) (PMMA); the structure height was increased by plasma etching [15–18]. In addition, the self-assembly of aluminum nanoholes also demonstrated antireflection properties [19, 20]. Because antireflection is achieved with a single layer of SWS, structure transfer processes can be used, such as UV nanoimprinting, hot embossing, or injection molding [21–23]. In considering the feature sizes of SWSs depending on optical characteristic and polymer filling, nanostructures of a small size are better for achieving these optical characteristics. However, polymer filling becomes more difficult for smaller structures. In contrast, for large-sized nanostructures, polymer filling is easily achieved by structure transfer process. However, the antireflective characteristics are decreased, and the optical transmittance is also decreased by scattering effects. The size of the nanostructure is negatively correlated with the SWS optical properties and forming characteristics. To obtain easy forming,

the UV nanoimprint process is an effective process, and the mold structure for the SWSs is easy to understand because the viscosity of the UV resin is very low; therefore, SWS mold filling is easy. In addition, the SWS mold structure is also easy to understand when the pattern transfer process uses heating and cooling, like in hot embossing [19, 24–26]. In the heating process, the polymer resin almost completely fills the structure because the viscosity is lower when the polymer resin is fully melted. After cooling, the resin strength is high because of solidification of the polymer resin. However, the process cycle is long term because of the heating and cooling process. To achieve the process cycle in short term, the general injection molding process is expected because the mold temperature is constant, unlike in the hot-embossing process with heating and cooling process. Although the sizes and height of the nanostructures have to be controlled to obtain SWSs with good optical characteristics of low reflectance and high transmittance, the polymer filling in nanostructure is difficult because controlling the viscosity of the polymer is not easy for the injection molding process. For polymer injection into a nanostructured mold, the low polymer viscosity is effectively the same as that in the hot embossing or UV imprinting process. Although the viscosity of the polymer is decreased with increasing mold temperature, the mold temperature is limited because the polymer cannot solidify when the mold temperature exceeds the melting point of the polymer. Thus, investigations of the SWS optical properties and nanoforming characterization depending on the nanostructure size are important to better understand the fabrication of plastic optical components with SWS antireflection. In this study, we investigated the characteristic relationship between the SWS antireflectance and nanoforming by varying the nanostructure size to adapt to the production of plastic optical components.

2 Materials and methods

Figure 1 shows the fabrication process of the SWS mold using metallic nanoparticles [18]. First, lens molds are prepared (Figure 1A). A stainless steel mold of STAVAX (Uddeholm, Hagfors, Sweden), commonly used in injection molding, is employed as the base material. The STAVAX mold is fabricated as a lens shape using computerized numerical control (CNC) machining. Next, stacked silicon nitride and thin platinum oxidized layers are deposited on the mold by magnetron sputtering, with thicknesses of 450 nm and 8–12 nm, respectively. After deposition, the mold is annealed, causing the platinum oxidized layer to form metallic nanoparticles of platinum [27]. Here, by varying the thickness of the platinum oxidized layer, the metallic nanoparticle size is changed. The metallic nanoparticles remain on the mold, as shown in Figure 1C. After nanoparticle formation, the silicon nitride layer is etched by reactive ion etching (RIE) of the capacitive coupled plasma (CCP) type. The reactive gas of CF_4 is

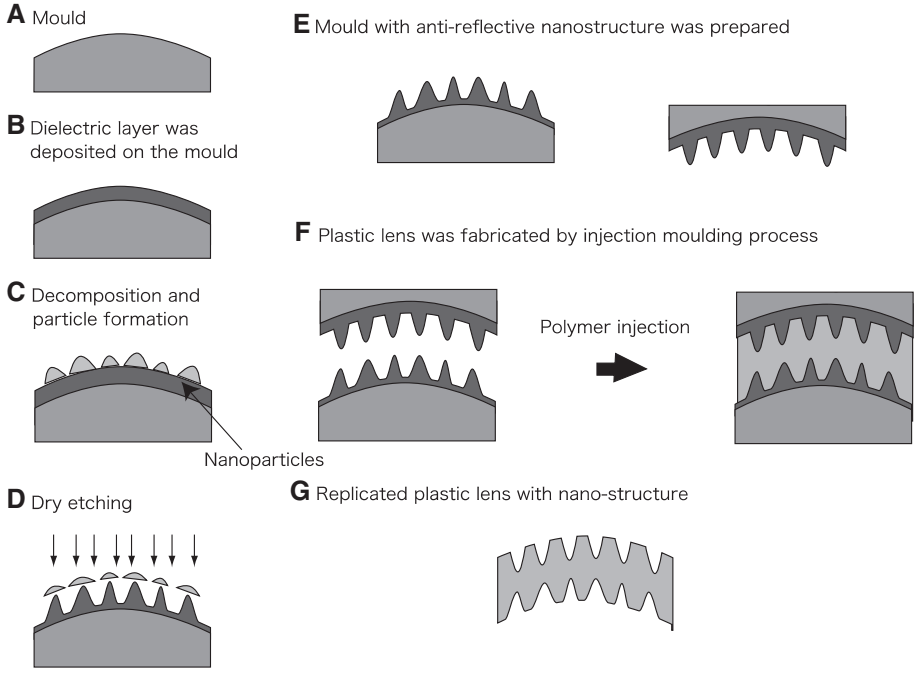

Figure 1: Fabrication process for the SWS mold using metallic nanoparticles.
(A) Lens molds are prepared, (B) stacked dielectric layer and thin metallic layers are deposited, (C) the mold is annealed and themetallic nanoparticles formation, (D) dielectric layer was etched, (E) mold with anti-reflective nanostrcture was prepared, (F) plastic lens was fabricated by injection moulding process, (G) replicated plastic lens with nanostructure was fabricated.

employed at the process pressure of 2 Pa. The etching power is set to 50 W. The metallic nanoparticles are also etched during the etching process because the metallic nanoparticles are a sacrificial layer. To remove the metallic particles completely, the reactive gas is changed from CF_4 to Ar. The etching selectivity ratio between the silicon nitride and the metallic nanoparticle was changed by this change in reactive gas. Finally, a 400-nm-high SWS on the silicon nitride layer is fabricated on the lens mold, as shown in Figure 1E. Here, according to a previous research report, a fluorine monolayer is generally coated on the mold surface to allow easy separation. In this experiment, no additional coating is employed. The utilized cyclo-olefin polymer (COP; Zeonex 480R) has hydrophobic properties with a contact angle of 97.9° with 1-µl water droplets. In addition, the combinations of the COP and the silicon nitride SWSs are easily separated. In the mold fabrication preparation, only dry processes are used, so the curved SWS molds are easily created. After preparing the SWS mold, the plastic lens is replicated by injection molding, as shown in Figure 1F. The plastic lens and SWS are replicated simultaneously, as shown in Figure 1G. Finally, antireflective characteristics emerge from the SWS on the plastic lens.

3 Results and discussion

Figure 2 shows the average particle diameter and atomic force microscope (AFM) images. Figure 2A–C shows images of metallic nanoparticles from films of 8 nm, 10 nm, and 12 nm in thickness, respectively. The AFM images of the nanoparticles are measured on the mold during the SWS fabrication process. By varying the thickness of the metallic film, the diameter of the metallic nanoparticles is changed. The particle size reproducibility is stable because the metal thickness controllability is approximately ±1.5 Å for metallic thin-film deposition by magnetron sputtering.

The average diameters of the metallic nanoparticles are 83.8 nm, 111.2 nm, and 112.3 nm, and the dispersions 3σ are 48.9 nm, 72.1 nm, and 81.4 nm, for the metal films of different thicknesses, such as MT8, MT10, and MT12 for the 8-, 10-, and 12-nm-thick films, respectively. By increasing the deposited metal thickness, the maximum diameter of the nanoparticles is increased; thus, the space between nanoparticles is also increased. After metallic nanoparticle formation, each mold is etched by RIE. The nanostructure heights of the molds, as measured by AFM, are 390 nm, 378 nm, and 376 nm from the mold of MT8, MT10, and MT12, respectively.

The thermal properties of the polymer are important because nanostructure replication depends on the reliable melting and solidification of the polymer, as determined by the temperature of the mold. The melting point and glass transition temperature T_g vary for different polymer materials and grades. The thermal properties of COP are shown in Figure 3. The polymer melts gradually with an initial melting temperature of 123°C. The T_g is 140°C.

Figure 4 shows the variations in the nanostructure heights in relation to changes in the mold temperature with varied SWS patterns. In the nanostructure transfer process with the injection molding machine, the polymer is heated to >300°C in the cylinder. After melting, the melted polymer is injected into the mold and then solidified. The mold temperature is varied from 110°C to 150°C. The mold and nanostructure of the transferred polymer are then separated, and the nanostructure height is measured by AFM. For the Mold MT8, the nanostructure heights are gradually increased from 114 to 202 nm as the mold

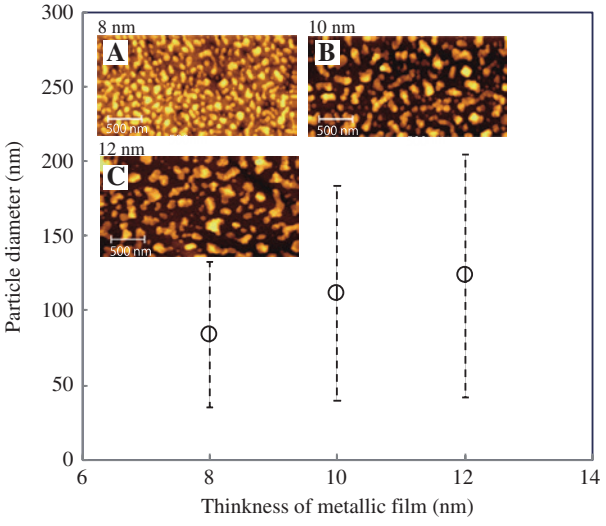

Figure 2: Relationship between metallic film thickness and nanoparticle diameter. Insets show AFM images of nanoparticles from metallic films of (A) 8 nm, (B), 10 nm, and (C) 12 nm in thickness.

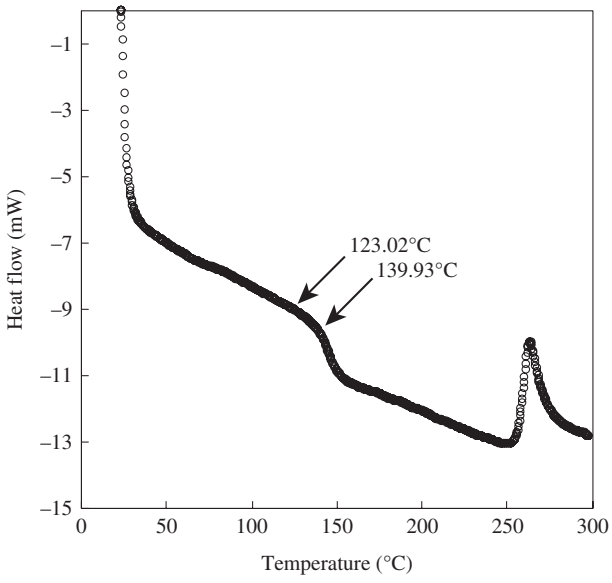

Figure 3: Differential scanning calorimetry curve of COP (Zeonex 480R).

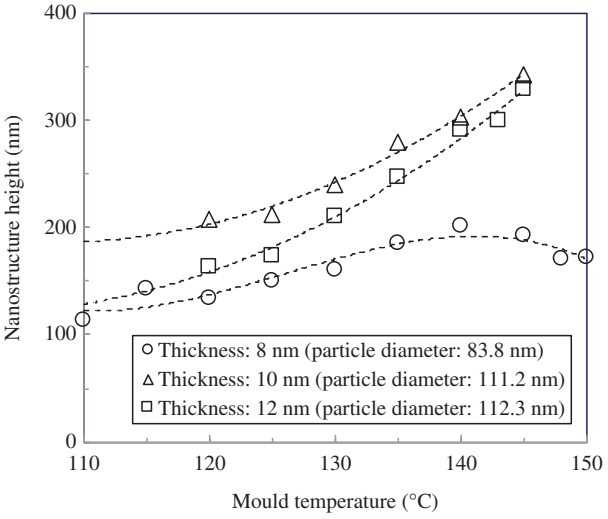

Figure 4: Variations in the nanostructure height relative to mold temperature.

temperature is increased from 110°C to 140°C. The nanostructure height of Mold MT8 was measured to be 390 nm. The filling rate was estimated to be 51.7% at a mold temperature of 140°C. However, the height of the nanostructure is gradually decreased from 202 nm to 170 nm at mold temperatures >140°C. We consider that a separation problem occurs between the mold and replicated polymer for Mold MT8 because the polymer is not sufficiently solidified. The strength of the polymer is decreased because the T_g of the polymer is 140°C, as shown in Figure 3. The number of particle per unit area is estimated at 53.25 μm^2, 28.4 μm^2, and 22.19 μm^2 for Molds MT8, MT10, and MT12, respectively. The contact interface area between the nanostructure and injected polymer is defined by multiplying the outer circumference of the average particle diameter, the number of particle per unit area, and the height (h) of the filled polymer in the mold. The contact interface areas between the nanostructures and injected polymers are estimated to be 14.0(h), 9.9(h), and 8.6(h) from MT8, MT10, and MT12, respectively. The contact interface area for Mold MT8 is 1.4–1.6 times higher than those for Molds MT10 and MT12. Therefore, we attribute the separation problem to the increased bonding strength from Mold MT8 relative to those of the other mold. For the Molds MT10 and MT12, the nanostructure height from Mold MT10 is gradually increased from 208 nm to 342 nm as the mold temperature is increased from 120°C to 145°C. The nanostructure heights are measured to be 378 nm and 376 nm from Molds MT10 and MT12, respectively. The filling rates of MT10 and MT12 were estimated to be 90.4% and 87.8%, respectively, at the mold temperature of 145°C. In comparing the polymer filling rates of Molds MT8 and MT10 at the mold temperature of 140°C, the filling rate was increased from 51.7% to 73.7% at the same processing condition. We consider that decreasing the particles density was effective to allow polymer filling. The space areas for polymer filling calculated from the particle density for Molds MT10 and MT12 were expanded 1.8–2.4 times compared to that from Mold MT8. Additionally, we believe that the space variation was an effective parameter for polymer filling based on the state changes in the growth of the polymer solidification layer distribution and the changes in exiting air by varying the nanostructure spacing. Overall, the polymer filling and separation phenomena are dramatically changed by varying the nanostructure size.

Figure 5 shows the antireflective property of a replicated plastic substrate relative to the mold temperature by each mold. Figure 5A and B shows the antireflective properties of the Molds MT8 and MT10, respectively. Figure 5C compares the antireflective properties achieved with various SWS with Molds MT8, MT10, and MT12, respectively, under the condition with a mold temperature of 138°C. The reflectance of both surfaces is measured. The flat surface without nanostructures shows the optical reflectances of 8.2% and 8.9% under wavelengths of 550 nm and 980 nm, respectively. With increasing mold temperature, the optical reflectance is decreased in order to increase the nanostructure height. For the SWS with Mold MT8, the reflectance is decreased to 0.84% under 550-nm wavelength at a mold temperature of 140°C. The valley of the reflectance is shifted to longer wavelengths as the nanostructure heights are increased. However, the reflectance is increased for mold temperatures of >140°C because the nanostructure heights are decreased by the mold separation problem. In contrast, with the SWS with Mold MT10, the reflectance is decreased to 0.93% under a wavelength of 980 nm at a mold temperature of 140°C. This indicates that the valley of reflectance is moved from the visible range to the near-infrared range by changing the SWS mold pattern as shown in Figure 5C. For an SWS with varied feature diameters and equal nanostructure heights of 200 nm, the optical reflectance is increased from 0.84% to 2.2% at a wavelength of 550 nm (in detail, the SWSs with the Molds MT8 and MT10 are obtained at mold temperatures of 140°C and 120°C, respectively). We consider that the reflectance increase is caused by the Mie scattering effect from variations in the maximum particle size parameter, calculated by the average diameter and the standard deviation. According to the Mie theory, the scattering distribution from the size parameter χ is determined by equation (1):

$$\chi = 2\pi r/\lambda \tag{1}$$

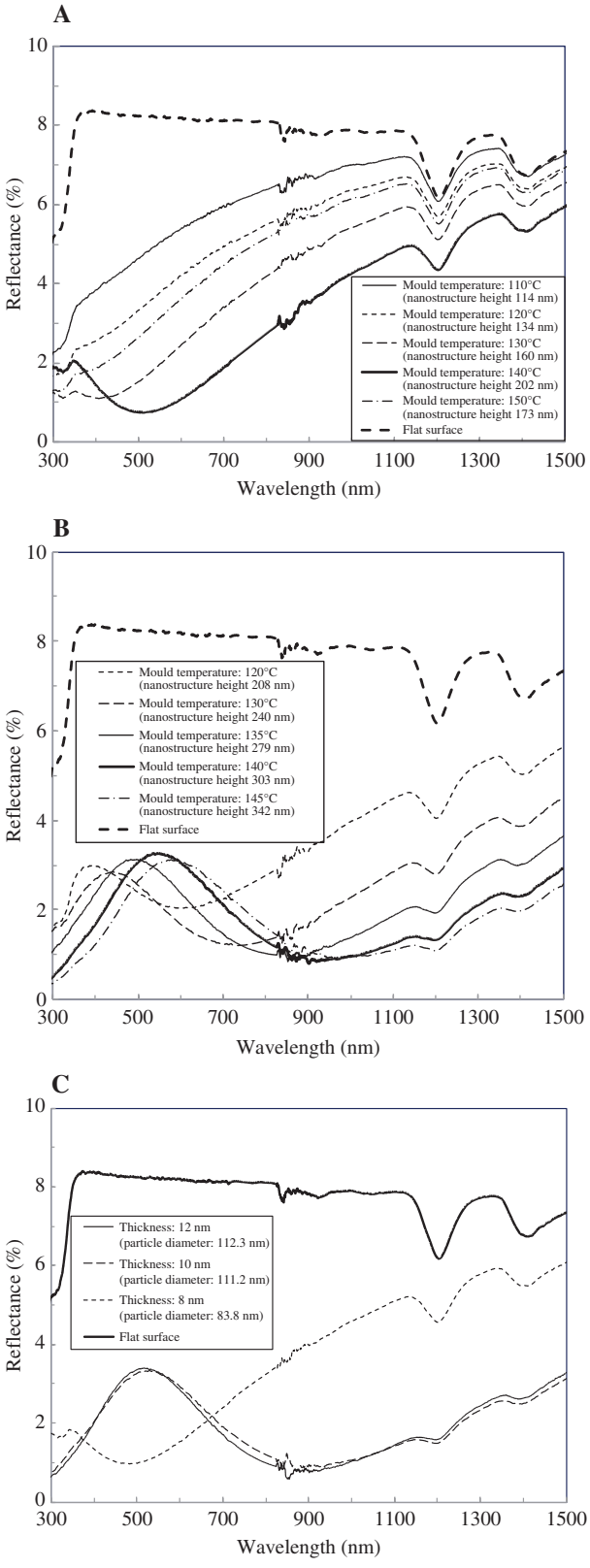

Figure 5: Reflectance and structure height in (A) 8-nm metal film thickness (Mold MT8) and (B) 10-nm metal film thickness (Mold MT10), and (C) reflectance by each SWS.

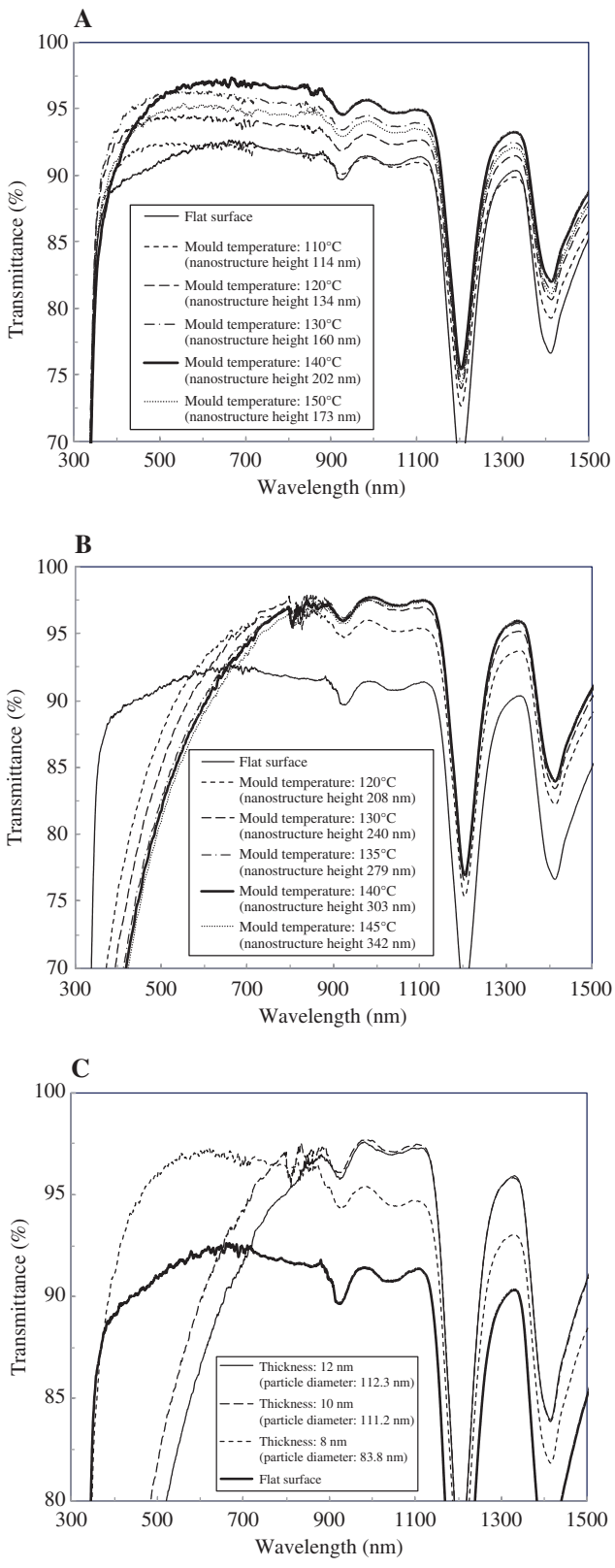

Figure 6: Transmittance and structure height in (A) 8-nm metal film thickness (Mold MT8) and (B) 10-nm metal film thickness (Mold MT10), and (C) transmittance by each SWS.

Here, r is the particle radius, and λ is the wavelength. For the size parameter χ over 1, forward scattering is greater than backscattering. At a wavelength of 550 nm, particle diameters of >175 nm yield the size parameter χ larger than 1. As the maximum particle diameter of the SWS with Mold MT10 is 205 nm, we consider that the forward scattering effect is increased; thus, the SWS reflectance at a wavelength of 550 nm is also increased. Figure 6 shows the optical transmittance in relation to the mold temperature for varying SWS patterns. Figure 6A and B shows the optical transmittances of the SWS with Molds MT8 and MT10, respectively. Figure 6C shows the comparison of the optical transmittance with changes in the SWS Molds MT8, MT10, and MT12, respectively. For the flat surface without nanostructures, the transmittance is 91.7% and 91.4% under wavelengths of 550 nm and 980 nm, respectively. For the SWS with Mold MT8, the optical transmittance is increased as the mold temperature is increased. The transmittance is 96.6% at 550 nm for a mold temperature of 140°C. The variations in the optical transmittance spectra correspond to those of the reflectance spectra. Even for SWSs of different feature sizes, the optical transmittance increases with increasing nanostructure height. However, by increasing the particle diameter, as shown in Figure 6C, the optical transmittance is clearly decreased, while the wavelength is shifted to shorter wavelengths by the Mie scattering effect. By increasing the nanostructure height, the Mie scattering effect is increased at shorter wavelengths. We consider that the nanostructures in the vertical direction affect the Mie scattering for structures of horizontal dimensions fulfilling the size parameter χ of the Mie theory. Overall, the size of the SWS determined the optical properties and the nanoforming characteristics. The SWS must be clearly controlled in the parameter of the structure height and size to achieve antireflectance under certain optical wavelengths by the injection-molding process.

4 Conclusions

The effects of SWS size on the antireflectance properties and nanomolding characteristics were investigated. Several molds based on metallic nanoparticles were prepared with average nanoparticle diameters of 83.8 nm, 111.2 nm, and 112.3 nm, and structure heights of 390 nm, 378 nm, and 376 nm, respectively. Polymer filling and separation in the nanostructures were related to the particle mask size of the SWS. For the phenomenon of polymer separation problems in the structure, the bonding strength varied depending on the surface area ratio; that of the smallest nanoparticle was 1.6 times larger than that of the large-sized particles. In addition, maximum polymer filling varied with changing SWS feature sizes; structures with larger spacing were more easily filled, with the packing ratio increased from 51.7% to 90.4% when the space area between nanostructures was expanded 1.8–2.4 times compared to the smallest spacing. In addition, the filled ratio of the injected polymer was increased from 51.7% to 73.7% at a constant mold temperature of 140°C by expanding the space area calculated from particle density. This effectively changed the growth of the polymer solidification layer distribution and the exiting air. Thus, the filling and separation phenomena were dramatically affected by the nanostructure size. In analyzing the optical properties of the SWS, the reflectance was decreased to 0.84% at a wavelength of 550 nm with an average feature diameter and mold temperature of 83.8 nm and 140°C, respectively. In contrast, for the SWS with features of 111.2 nm in average diameter, the reflectance was decreased to 0.93% at a wavelength of 980 nm and a mold temperature of 140°C. This indicated that the valley of the reflectance was moved from the visible range to the near-infrared range by changing the SWS mold pattern, even though the mold temperature was constant. This result led us to conclude that we can obtain antireflection surfaces for any wavelength by varying the size of the SWS under the same injection molding condition.

References

[1] G. C. Par, Y. M. Song, J.-H. Ha and Y. T. Lee, J. Nanosci. Nanotechnol. 11, 6152–6156 (2011).
[2] C.-H. Sun, P. Jiang and B. Jiang, 92, 061112 (2008).
[3] T. Tamura, M. Umetani, K. Yamada, Y. Tanaka, K. Kintaka, et al., Appl. Phys. Express 3, 112501 (2010).
[4] J.-H. Shin, H.-J. Choi, G.-T. Kim, J.-H. Choi and H. Lee, Appl. Phys. Express 6, 055001 (2013).
[5] T. Glaser, A. Ihring, W. Morgenroth, N. Seifert, S. Schröter, et al., Microsyst. Technol. 11, 86–90 (2005).
[6] B. Päivänranta, T. Saastamoinen and M. A. Kuittinen, Nanotechnology 20, 375301 (2009).
[7] J. Turunen, in 'Micro-Optics', Ed. By H. P. Herzig (Taylor & Francis, London, 1998).
[8] K. Forberich, G. Dennler, M. C. Scharber, K. Hingerl, T. Fromherz, et al., Thin Solid Films 516, 7167–7170 (2008).
[9] S. Ji, J. Park and H. Lim, Nanoscale 4, 4603–4610 (2012).
[10] D.-H. Ko, J. R. Tumbleston, K. J. Henderson, L. E. Euliss, J. M. DeSimone, et al., Soft Matter 7, 6404–6407 (2011).
[11] J. Sun, X. Wang, J. Wu, C. Jiang, J. Shen, et al., Sci. Rep. 8, 5438 (2018).
[12] H. Jung and K.-H. Jeong, Appl. Phys. Lett. 101, 203102 (2012).

[13] D. H. Macdonald, A. Cuevas, M. J. Kerr, C. Samundsett, D. Ruby, et al., Sol. Energy 76, 277–283 (2004).
[14] H. H. Solak, J. Phys. D: Appl. Phys. 10, R171–R188 (2006).
[15] R. Ruiz, H. Kang, F. A. Detcheverry, E. Dobisz, D. S. Kercher, et al., Science 321, 926–939 (2008).
[16] E. Han, K. O. Stuen, Y.-H. La, P. F. Nealey and P. Gopalan, Macromolecules 41, 9090–9097 (2008).
[17] C.-C. Liu, P. F. Nealey, Y.-H. Ting and A. E. Wendt. J. Vac. Sci. Technol., B. 25, 1963–1968 (2007).
[18] B. Päivänranta, P. K. Sahoo, E. Tocce, V. Auzelyte, Y. Ekinci, et al., ACS Nano 5, 1860–1864 (2011).
[19] T. Yanagishita, M. Masui, N. Ikegawa and H. Masuda, J. Vac. Sci. Tech. B 32, 021809 (2014).
[20] T. Yanagishita, T. Hidaka, M. Suzuki and H. Masuda, J. Vac. Sci. Tech. B 34, 021804 (2016).
[21] Y. Kanamori, M. Okochi and K. Hane, Opt. Express 21, 322–328 (2013).
[22] B.-J. Bae, S.-H. Hong, E.-J. Hong, H. Lee and G. Y. Jung, Jpn. J. Appl. Phys. 48, 010207 (2009).
[23] I. Mano, T. Uchida and J. Taniguchi, Microelectron. Eng. 191, 97–103 (2018).
[24] C. David, P. Haberling, M. Schnieper, J. Sochtig and C. Zschokke, Microelectron. Eng. 61–62, 435–440 (2002).
[25] S. S. Oh, C.-G. Choi and Y.-S. Kim, Microelectron. Eng. 87, 2328–2331 (2010).
[26] Q. Chen, G. Hubbard, P. A. Shields, C. Liu, D. W. E. Allsopp, et al., Appl. Phys. Lett. 94, 263118 (2009).
[27] K. Kurihara, Y. Saitou, N. Souma, S. Makihara, H. Kato, et al., Mater. Res. Express 2, 015008 (2015).